Dimorphism of Hepatitis B Virus Capsids Is Strongly Influenced by the C-Terminus of the Capsid Protein

A. Zlotnick,[‡] N. Cheng,[‡] J. F. Conway,[‡] F. P. Booy,[‡] A. C. Steven,*[,‡] S. J. Stahl,[§] and P. T. Wingfield[§]

Laboratory of Structural Biology and Protein Expression Laboratory, National Institute of Arthritis, Musculoskeletal and Skin Diseases, National Institutes of Health, Bethesda, Maryland 20892

Received February 27, 1996; Revised Manuscript Received April 3, 1996[⊗]

ABSTRACT: Hepatitis B virus (HBV) is an enveloped virus with an icosahedral capsid. Its homodimeric capsid protein ("core antigen") assembles into particles of two sizes, one with $T = 3$ icosahedral symmetry (90 dimers) and the other with $T = 4$ symmetry (120 dimers). We have investigated this assembly process *in vitro*, using a variety of purified, bacterially expressed, capsid proteins. All of our constructs lacked the predominantly basic C-terminal 34 amino acids of the full-length capsid protein (183 amino acids) and were further truncated to terminate at specific points between residues 138 and 149. While the smallest construct (138 residues) did not assemble into capsids, those terminating at residue 140, and beyond, assembled into mixtures of $T = 3$ and $T = 4$ particles. The two kinds of capsids could be separated on sucrose gradients and did not interconvert upon protracted storage. The proportion of $T = 3$ capsids, assayed by sucrose gradient fractionation, analytical ultracentrifugation, and cryoelectron microscopy, was found to increase systematically with larger deletions from the C-terminus. The variant terminating at residue 149 formed ∼5% of $T = 3$ capsids, while the 140-residue protein produced ∼85% of this isomorph. For the 147-residue capsid protein, the structures of both capsids were determined to 17 Å resolution by three-dimensional reconstruction of cryoelectron micrographs. In these density maps, the boundaries of the constituent dimers can be clearly seen and the quaternary structures of the two capsids compared. The arrangement of dimers around their icosahedral five-fold axes is almost identical, whereas the quasi-six-fold arrangements of dimers are distinctly different.

Hepatitis B virus (HBV),[1] the archetypal Hepadnavirus, is a causative agent of viral hepatitis, cirrhosis of the liver, and hepatocellular carcinoma. There are estimated to be up to 500 million cases of chronic HBV infection, worldwide. The vaccines available for HBV do not always yield an immune response: likewise, therapy for chronic infection is not always effective (Hollinger, 1990; Nassal & Schaller, 1993). An improved understanding of the structure and assembly of the virus may provide a basis for developing new antiviral therapies.

HBV is a small DNA virus with a lipid−protein envelope surrounding an icosahedral capsid [for reviews, see Ganem and Varmus (1987) and Robinson (1991)]. The capsid plays a vital role in the unusual life cycle of this virus. Capsid assembly takes place in the cytoplasm and is initiated around a complex of viral mRNA and HBV reverse transcriptase. The enzyme becomes active in the assembled capsid, retrotranscribing the partially double-stranded DNA genome from the mRNA and digesting the mRNA template (Summers & Mason, 1982; Bartenschlager & Schaller, 1992).

Two variants of the capsid (or "core") protein are expressed by the same gene from different in-frame initiation codons. The gene product initiated at the second methionine codon is the serologically defined c-antigen, HBcAg. This protein has an arginine-rich, histone-like, C-terminus that is required for packaging nucleic acids (Petit & Pilot, 1985). The other gene product includes a signal sequence and is subject to proteolytic processing: 19 of the 29 additional N-terminal amino acids and 34 residues from the C-terminus are removed, resulting in a 159 amino acid protein, the e-antigen, HBeAg (Takahashi et al., 1983). In this study, we have generated and studied the variants of the latter protein listed in Figure 1.

Both HBcAg and HBeAg have been expressed in *Escherichia coli* where they assemble into capsids (Stahl et al., 1982; Cohen & Richmond, 1982; Murray, 1987; Crowther et al., 1994; Wingfield et al., 1995). These capsids are morphologically similar to native capsids (Kenney et al., 1995) and have similar antigenic properties. HBcAg capsids incorporate bacterial nucleic acids (Pasek et al., 1979) and are remarkably stable (Wingfield et al., 1995). Cpe protein, a close analog of HBeAg, forms empty particles which can be dissociated into dimers without unfolding the protein and reassembled under appropriate conditions (Wingfield et al., 1995).

Physicochemical studies of HBV capsids and dissociated capsid protein have revealed some unusual properties. (i) Cpe and HBeAg are ∼65% α-helical, both as dissociated dimers and in assembled capsids (Zheng et al., 1992; Wingfield et al., 1995). HBcAg has a slightly lower helical content, attributable to a nonhelical C-terminus. Accordingly, the fold of these proteins must be different from the

* Corresponding author: Building 6, Room 425, National Institutes of Health, Bethesda, MD 20892-2755. Phone: (301) 496-0132. Fax: (301) 402-3417. E-mail: Alasdair_Steven@nih.gov.

[‡] Laboratory of Structural Biology.

[§] Protein Expression Laboratory.

[⊗] Abstract published in *Advance ACS Abstracts,* May 15, 1996.

[1] Abbreviations: AEBSF, 4-(2-aminoethyl)benzenesulfonylfluoride; Cp, capsid protein; CTF, contrast transfer function; DTT, dithiothreitol; EDTA, ethylenediaminetetraacetic acid; FEG, field emission gun; FRC, Fourier ring correlation; HBcAg, hepatitis B core antigen; HBeAg, hepatitis B e antigen; HBV, hepatitis B virus; IPTG, isopropyl β-D-thiogalactopyranoside; PFT, polar Fourier transform; SDS−PAGE, sodium dodecyl sulfate−polyacrylamide gel electrophoresis.

S0006-2960(96)00480-1

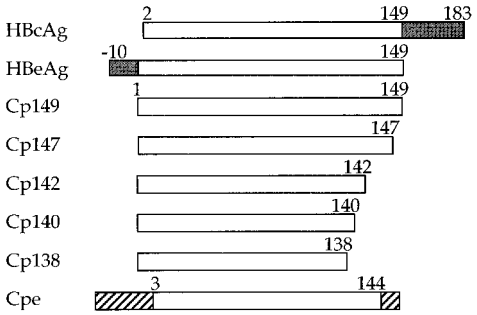

FIGURE 1: HBV capsid protein (Cp) constructs. The additional N-terminal (HBeAg) and C-terminal (HBcAg) sequences are shaded. Amino acids 139−149, where the truncations to the Cp proteins have been made, are ILSTLPETTVV. All of the Cp protein constructs, except Cpe, include the N-terminal methionine which is absent from native HBcAg. The N- and C-termini of Cpe are TMITDSLEFHI and IS (diagonal lines), respectively, and are remnants of the cloning vector. The protein construct Cp149 C61A is identical in sequence to Cp149 except that cysteine 61 is mutated to alanine.

canonical eight-stranded β barrel, which is the basic motif of virtually all capsid proteins of icosahedral viruses whose structures have been solved to date (Rossmann & Johnson, 1989; Stuart, 1993). (ii) While most viral capsid proteins assemble into particles of a fixed, predetermined size, HBV capsids are dimorphic. As shown by cryoelectron microscopy (Crowther et al., 1994) and scanning transmission electron microscopy (Wingfield et al., 1995), there are two size variants: a smaller capsid with a triangulation number (Caspar & Klug, 1962) of $T = 3$, and a larger capsid with $T = 4$ (Figure 2).

The factors which control the dimorphic switch are not understood. Nor are the physiological implications of this phenomenon clear, although the $T = 4$ form is reported to outnumber the $T = 3$ form by ~13 to 1 in capsids isolated from human liver (Kenney et al., 1995). This study was undertaken to gain some insight into the structural and physicochemical basis of HBV capsid assembly and polymorphism. We have worked with highly purified capsid proteins (Cp), assembled under standardized conditions. Noting that the $T = 4/T = 3$ ratio appears to be affected by the presence of the basic C-terminus and encapsidated nucleic acid (Crowther et al., 1994; Wingfield et al., 1995), we developed a series of progressively longer C-terminal deletions [see Birnbaum and Nassal (1990) and Beames and Landford (1993)]. Sucrose gradients were used to separate $T = 3$ and $T = 4$ capsids. We used this technique in conjunction with electron microscopy and analytical ultracentrifugation to evaluate the relative proportions of $T = 3$ and $T = 4$ capsids in each preparation studied. Image reconstructions from cryoelectron micrographs were performed with the goal of identifying any conformational differences between the capsid protein dimers, as deployed in the two kinds of capsids, that are discernible at the currently accessible resolution.

MATERIALS AND METHODS

Construction of HBV Capsid Protein Genes. Cpe was produced using ptacHBc144, which was constructed from ptacHpaII (Stahl & Murray, 1989) by digesting this plasmid with *Hin*dIII, treatment with the Klenow fragment of DNA polymerase I and the four dNTPs, and recircularization of the plasmid with T4 DNA ligase. The DNAs encoding the

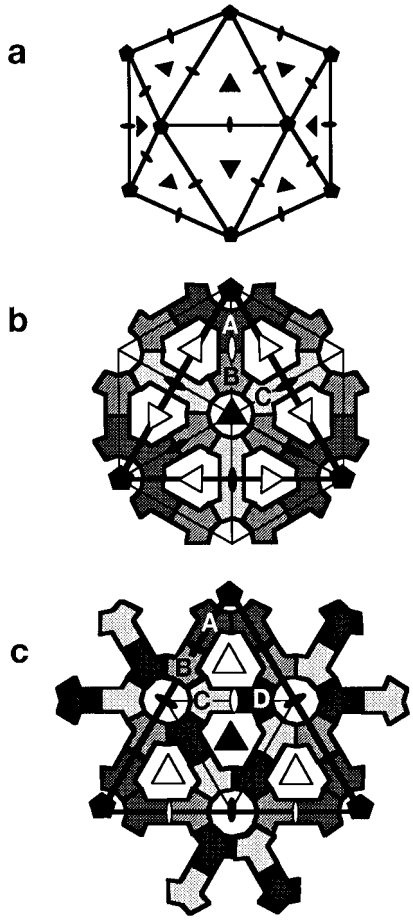

FIGURE 2: Icosahedral symmetry [see Caspar and Klug (1962)] and the arrangement of dimers in $T = 3$ and $T = 4$ icosahedra. (a) An icosahedron has 532 symmetry and is constructed from 20 equilateral triangles (facets). Five-fold symmetry axes (marked by pentagons) are found at the 12 vertices, two-fold axes (ovals) at the centers of the 30 edges, and three-fold axes (triangles) at the centers of the 20 facets. (b) A triangular facet for a $T = 3$ icosahedron composed of dimers. The 180 subunits in a $T = 3$ particle (each a half-dimer) occupy three distinct quasiequivalent environments, A, B, and C. There are 60 AB and 30 CC dimers, with the CC dimers located on icosahedral two-fold axes. The quasi-six-fold axes coincide with the icosahedral three-fold axes. Quasi-two-fold and quasi-three-fold axes are identified by open symmetry operator symbols, and icosahedral symmetry operators by filled symbols. (c) A facet of a $T = 4$ icosahedron composed of dimers. The four distinct quasiequivalent environments result in two types of dimer, AB and CD, 60 of each. In this case, the quasi-six-fold axes coincide with the icosahedral two-fold axes. The subunits in the triangular facets shown in b and c are to the same scale as the $T = 1$ icosahedron shown in a.

Cp138, Cp140, Cp142, Cp147, Cp149, and Cp149 C61A proteins were generated as *Nde*I−*Bam*HI fragments using PCR as described (Scharf et al., 1986) and cloned into the expression vector pET-11a (Studier et al., 1990).

The lengths of different genetic constructs are reflected in their names (Figure 1). Thus the protein extending from residue 1 to 149 is Cp149. The exception to this convention is Cpe, which has a native sequence from residue 3 to 144, a sequence derived from a cloning vector for residues −9 to 2, and two nonnative residues on its C-terminus (Figure 1).

Protein Purification. Plasmids were transformed into *E. coli* DE3 cells and grown at 37 °C in complex media of double strength LB medium containing 2−4% glucose, trace elements, and 200 μg/mL carbenicillin in a 2-L Biostat MD fermentor (Braun Biotech Inc., Allentown, PA). Protein

expression was induced with 2 mM IPTG for 3 h at 37 °C. About 60−80 g wet weight of cells was obtained. SDS−PAGE indicated that HBV protein represented 5−15% of the total *E. coli* protein. Cells were resuspended in 200 mL of 50 mM Tris-HCl, pH 7.4, containing 1 mM EDTA, 5 mM DTT, 1 mM AEBSF (Pefabloc SC supplied by Boehringer, Indianopolis, IN), 0.1 mg/mL RNase, and 0.1 mg/mL DNase 1 (both nucleases originated from bovine pancreas and were supplied by Fluka, Ronkokoma, NY). The cells were lysed by one pass through a French pressure cell operated at 16 000 psi. The suspension was briefly sonicated and then centrifuged at 26000*g* for 1 h. Solid sucrose was added to the supernatant to a concentration of 0.15 M and then recentrifuged at 100000*g* for 1 h. Solid $(NH_4)_2SO_4$ was slowly added to the supernatant to a final concentration of 40% saturation. The solution was gently stirred for 1 h after which it was centrifuged at 26000*g* for 1 h. The pellet was resuspended with 50−60 mL of 100 mM Tris-HCl, pH 7.5, 100 mM NaCl, 50 mM sucrose, and 2 mM DTT (column buffer A) and loaded on a Sepharose CL-4B (Pharmacia Biotech, Piscataway, NJ) column (5 cm diameter × 95 cm) equilibrated with column buffer A. The column was eluted at 2 mL/min. HBV capsids were well separated from large aggregates (which eluted in the void volume) and from soluble proteins of lower molecular weight. Fractions were pooled on the basis of the chromatographic profile and SDS−PAGE and then concentrated by ultrafiltration using a Diaflo YM 100 ultrafiltration membrane (Amicon, Beverly, MA) to about 10 mg/mL. Concentrated protein was dialyzed against 50 mM Tris-HCl, pH 7.5, containing 0.15 M sucrose. About 300 mg of dialyzed protein (∼30 mL; unused capsids were stored at −80 °C) was titrated to pH 9.5 with 10 N NaOH, solid urea added to 3.5 M, and the solution volume adjusted to 50 mL with water. The solution containing dissociated capsids was filtered using a Millex-HA 0.45-μm pore size filter unit (Millipore, Bedford, MA) and applied to a column (6.0 cm diameter × 60 cm) of Superdex 75 (Pharmacia Biotech, Piscataway, NJ) equilibrated with 100 mM sodium bicarbonate, pH 9.5, containing 2 mM DTT. The column was eluted at 5 mL/min and fractions containing dimeric protein were pooled on the basis of SDS−PAGE analysis. The yield of purified HBV dimer was 3−10 mg per g wet weight of starting cells.

Protein was quantified by absorbance at 280 nm using extinction coefficients of $\epsilon^{mg/mL}$ of 1.69 cm^{-1} for Cpe, 1.74 cm^{-1} for Cp149 and Cp149 C61A, 1.77 cm^{-1} for Cp147, 1.84 cm^{-1} for Cp142, and 1.86 cm^{-1} for Cp140.

Capsid Assembly and Separation. Capsids were assembled at 20 °C either by dialysis of a stock of dimer (0.8−2.4 mg/mL) in 0.1 M bicarbonate buffer, pH 9.5, against 0.1 M HEPES and 0.2−0.5 M NaCl, pH 7.5, or by mixing with a more concentrated buffer (typically a 2:1 dilution with 0.15 M HEPES and 0.3 M NaCl, pH 7.5).

$T = 3$ and $T = 4$ particles were separated on 5−30% sucrose gradients buffered with 0.1 M HEPES and 0.2 M NaCl, pH 7.5. Gradients were made by tilted rotation (Coombs & Watts, 1985) using a Gradient Master (Biocomp, Fredericton, NB). For SW40 tubes (all centrifuge tubes and rotors were Beckman, Palo Alto, CA) (13.5 mL), a maximum sample size of 400 μL (volume) or 0.5 mg (protein) was overlaid onto the gradient. Gradients were centrifuged at 200000*g* for 2 h in an SW40 swinging bucket rotor at 19 °C. Larger gradients, prepared in SW28 tubes (38.5 mL), were loaded with a maximum volume of 1 mL sample volume or 1.5 mg of protein and centrifuged for 4.5 h at 105000*g*. Bands were visualized by illuminating the gradient and collected by side puncture.

For investigating the concentration dependence of assembly, capsids were assembled by the mixing method. Samples (0.2 mg from a 20 mg/mL stock of dimer) were diluted to initial concentrations of 0.8, 4.0, and 10.0 mg/mL with 0.1 M sodium bicarbonate, pH 9.5, before being assembled by 1:3 dilution with 0.4 M HEPES and 0.8 M NaCl, pH 7.5. After 1 h at room temperature, the samples were concentrated using a Centricon 30 (Amicon, Beverly, MA) to a maximum volume of 300 μL before being loaded on to the gradient.

Analytical Ultracentrifugation. Analytical ultracentrifugation was carried out on a Beckman Optima XL-A instrument with an An-60 Ti rotor and standard double-sector centerpiece cells. Sedimentation velocity measurements were made at 20 000 rpm for 3 h at 20 °C with data collection every 10 min. Samples (∼0.5 mg/mL) were in 50 mM Tris HCl and 0.4 M NaCl, pH 7.5. Data were analyzed by the method of Stafford (1992), and peaks were analyzed using the peak fitting module of Origin (version 4.0, Microcal, Northampton, MA).

Electron Microscopy. For negative staining, capsids at 0.1−0.5 mg/mL protein were adsorbed to freshly glow-discharged, carbon-coated grids, washed with water, stained with 1% uranyl acetate, and observed in a Zeiss 902. For cryoelectron microscopy, vitrified thin films of capsids at 2−5 mg/mL in 50 mM HEPES and 100 mM NaCl, pH 7.5, were prepared as described by Booy et al. (1985, 1991), except that fenestrated carbon films were used as substrate. Micrographs were recorded at a nominal magnification of 38000× on a Philips CM20-FEG (Philips, Eindhoven, Netherlands), operating at 120 keV and equipped with a Gatan 626 cryoholder (Gatan, Pleasanton, CA). Dimensions were calibrated from cryomicrographs of capsids mixed with bacteriophage T4, whose tail has an axial spacing of 40.5 Å (Moody & Makowski, 1981). Low-dose techniques were employed, with each exposure corresponding to ∼5 $e^-/Å^2$. Two micrographs of each field were recorded at different focal settings (Toyoshima & Unwin, 1988). The closer-to-focus image was taken first to minimize the effect of radiation damage on its high resolution information. The micrographs were assessed for resolution and stigmation by optical diffraction of large areas, and their defocus values were estimated from the positions of the zeros of the contrast transfer function (CTF). For the focal pair used in the reconstructions described below, the first zeros lay at frequencies of $(\sim 17\ Å)^{-1}$ and $(28\ Å)^{-1}$, respectively.

Image Analysis and Reconstruction. Micrographs were digitized on a Perkin Elmer 1010MG microdensitometer at a rate corresponding to 3.4 Å per pixel. Particles were extracted and processed using the automated procedure of Conway et al. (1993). One hundred twenty $T = 4$ capsids and 101 $T = 3$ capsids were collected from both members of the focal pair. Data from the further-from-focus micrograph were used to calculate density maps at 44 Å resolution, after orientations and particle origins were identified by "common lines" procedures (Crowther, 1971; Fuller, 1987; Baker et al., 1988, 1989; Trus et al., 1992; Johnson et al., 1994). These maps provided starting points for more refined analyses with the Polar Fourier Transform (PFT) algorithm,

which performs a model-based search (Baker & Cheng, 1996). With the refined parameters, reconstructions were calculated to a resolution of ~33 Å ($n = 75$, $T = 3$; $n = 49$, $T = 4$). These maps then served as initial models for PFT analyses of the closer-to-focus micrograph, yielding reconstructions to 25 Å resolution.

In correcting for phase reversal and signal attenuation effects arising from the CTF, our overall strategy was similar to those of others (e.g., Unwin, 1993; Zhou et al., 1994). Specifically, we combined two differently focused micrographs to compensate for the weak signals in their respective Fourier transforms around the positions of the CTF zeros. The following expressions was used for the CTF, $C(\nu,\Delta f)$:

$$C[\nu,\Delta f] = A \sin(\gamma[\nu,\Delta f]) + B \cos(\gamma[\nu,\Delta f]) \qquad (1)$$

where

$$\gamma[\nu,\Delta f] = \frac{2\pi}{\lambda}\left[\frac{C_s\nu^4\lambda^4}{4} - \frac{\Delta f\nu^2\lambda^2}{2}\right] \qquad (2)$$

The phase shift γ is a function of ν, the spatial frequency, and Δf, the defocus. λ is the wavelength, and C_s, the coefficient of spatial aberration (Misell, 1978). This formalism assumes that there is no significant astigmatism, which was the case with the micrographs analyzed, as determined by optical diffraction. A and B are the proportions of phase and amplitude contrast, respectively. A, B, and Δf were determined by a systematic search to obtain the best least-squares fit for the positions of the first three zeros of the calculated CTF, compared to the values measured from optical diffraction patterns. The resulting value for B was 6%, in agreement with Toyoshima and Unwin (1988).

Next, a deconvolution operation was performed according to

$$F\,[\text{image}_{\text{corrected}}(\nu)] = \frac{F\,[\text{image}_1(\nu)] + F\,[\text{image}_2(\nu)]}{|C_1(\nu,f_1)| + |C_2(\nu,f_2)| + \Omega} \qquad (3)$$

Here, F [image(ν)] is the Fourier transform of an image, and Ω is a "Weiner" term (Banks, 1990), included to suppress numerical instability at frequencies close to CTF zeros of both micrographs. The particles' phase origins were determined in the preceding reconstructions, and a low-pass filter was imposed, eliminating data beyond $(10\ \text{Å})^{-1}$. Ω was set, by trial and error, to a value of 0.2. Because the low resolution Fourier terms were found to be anomalously strong [see Frank et al. (1995)], only the Fourier terms beyond the first maximum of the CTF were corrected. This decision was based on the assumption that, to a first approximation, the anomalous enhancement of the low-frequency terms compensates for their suppression by the CTF. Also, because these terms convey low resolution information, the details of the reconstruction are relatively insensitive to how they are handled.

New maps were calculated for both capsids using the CTF-corrected images and the previously determined orientations. The orientations and maps were progressively refined by multiple cycles of PFT. Many particles did not correlate with the model structures beyond 25 Å resolution, as assessed by their Fourier Ring Correlation Coefficients (FRC) (Saxton & Baumeister, 1982; Conway et al., 1993) and were discarded. Ultimately, 28 particles of $T = 3$ and 31 of $T = 4$ were deemed suitable for inclusion in the final reconstructions, whose resolution was 17 Å in both cases, as measured by FRC.

The $T = 3$ and the $T = 4$ reconstructions were contoured to include a volume equal to 100% of the protein, assuming a specific volume of 0.742 cm^3/g.

RESULTS

Assembly and Separation of $T = 3$ and $T = 4$ Particles. When Cpe, assembled by dialysis against 400 mM NaCl and 100 mM Tris-HCl, pH 7.5, was loaded on a Sepharose CL-4B column, almost all of the material eluted in a broad peak within the included volume. Electron microscopy showed this material to consist of mixed $T = 3$ and $T = 4$ capsids. Although they were not resolved, the early fractions were enriched in $T = 4$ particles and later fractions in the smaller $T = 3$ form. Under these conditions, polymerization of Cpe dimer was nearly quantitative (~95%). Very little material was in the form of large aggregates eluting in the void volume (<1%), and very little residual dimer was observed in a small peak (~4%).

When 0.5 mg of Cpe capsids assembled *in vitro* were run on 5−30% sucrose gradients, two closely spaced bands were resolved. The material isolated from each band was examined by negative staining and/or cryoelectron microscopy. The upper, slower migrating, band, which contained ~80% of the assembled protein, was found to contain almost exclusively $T = 3$ particles (e.g., Figure 3b), and the lower band, $T = 4$ particles (e.g., Figure 3c). A shallower gradient (10−20%) resulted in broader bands without improving the separation; on a steeper gradient (5−50%), the bands were less diffuse but too close to be separately extracted.

Separation of the $T = 3$ and $T = 4$ species was initially accomplished with capsids assembled from Cpe protein and later repeated with the other constructs listed in Figure 1. For all of the variants studied, the sedimentation rates for the $T = 3$ and $T = 4$ bands were indistinguishable. In some preparations, particularly for Cpe, small amounts of protein were found as dimers of capsids and other higher molecular weight bands.

These results were complemented by analytical ultracentrifugation (Figure 4). Analysis of velocity sedimentation experiments showed that the major boundary could be resolved into two components sedimenting at 40S and 45S, respectively. $T = 3$ and $T = 4$ capsids separated on sucrose gradients were observed to sediment as homogenous species with the appropriate $S_{20,w}$ values (Figure 4). For most preparations, less than 10% of the protein sedimented as unpolymerized dimer at 2.5S (Wingfield et al., 1995). In preparations that included dimers of capsids, an additional faster sedimenting component (65S) was observed.

Gradient-purified $T = 3$ and $T = 4$ particles remained stable for several weeks at 4 °C. When pure $T = 3$ or pure $T = 4$ capsids were reloaded on 5−30% sucrose gradients, they sedimented as single bands at the appropriate positions, with at most a very faint band present at the position of the other capsid form. The relative amount of the contaminating form of capsid did not change over at least 2 weeks. Thus, we observe no evidence of equilibration between the two species as assayed by sucrose gradients and electron microscopy.

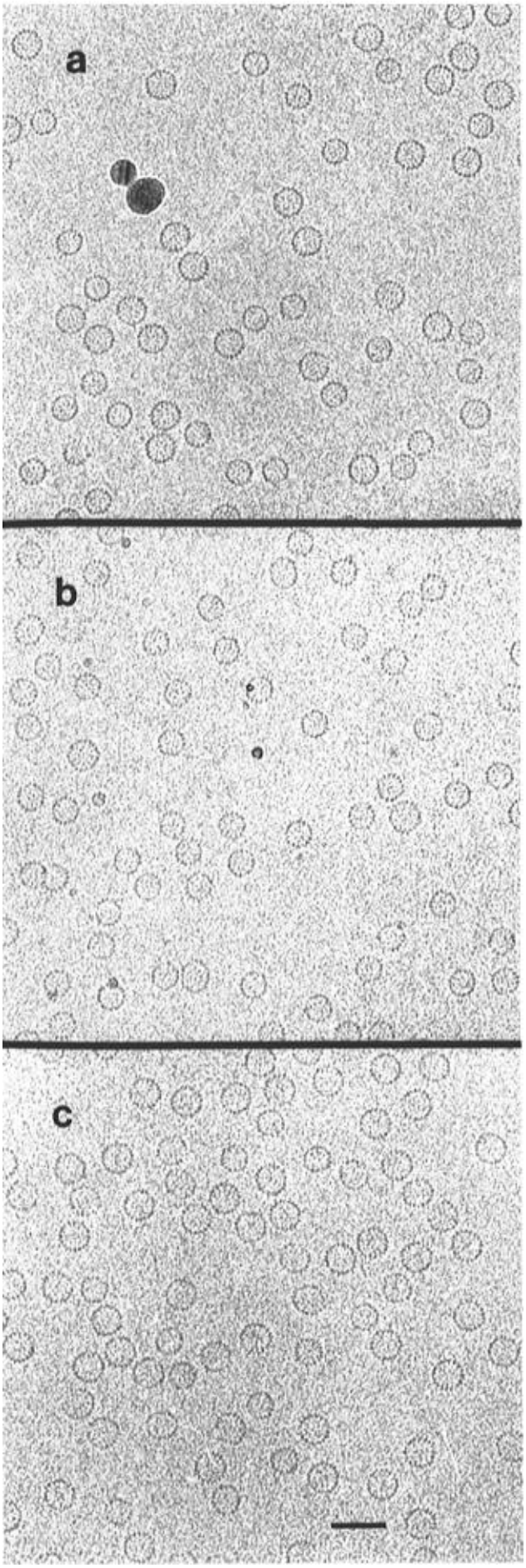

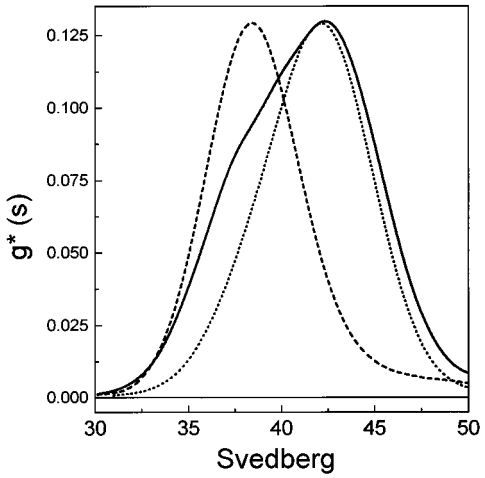

FIGURE 4: Sedimentation velocity of Cp142. Sedimentation analysis of unfractionated Cp142 (—) and $T = 3$ (— — —) and $T = 4$ (- - -) capsids purified by sucrose density centrifugation was performed according to Stafford (1992). The Cp142 sample is 40:60 $T = 3/T = 4$ capsids by absorbance. After correction for the relative number of subunits in each particle (see Table 1) this results in a 40:45 ratio or 53% $T = 4$ capsids. The $T = 4$ capsid sample used in this experiment included ~10% $T = 3$ capsids resulting in a broader peak that appears slightly shifted to lower *S* values. This experiment was performed with the same Cp142 sample used for the micrographs in Figure 3. The ordinate, $g^*(s)$, is the apparent sedimentation coefficient distribution and is not corrected for the effects of diffusion. The abscissa is Svedbergs (*S*) and has the units 1×10^{-13} s. The corrected sedimentation coefficients ($S_{20,w}$) of the Cp142 $T = 3$ and $T = 4$ species were 40*s* and 45*s*, respectively, and were separately determined by the transport method (Schachman, 1959).

Influence of C-Terminal Truncations on Capsid Assembly. To allow a systematic examination of the effect of the C-terminus on capsid assembly, we produced a series of C-terminal truncations (Figure 1). Of these, Cp149, Cp147, Cp142, and Cp140 all assembled into mixtures of $T = 3$ and $T = 4$ particles. However, further reducing the capsid protein by two residues (Cp138) removed the capability to assemble into capsids. The proportions of the two capsid isoforms were determined for each construct from the amounts of protein in the corresponding bands resolved on sucrose gradients (Table 1), by analysis of velocity sedimentation experiments in an analytical ultracentrifuge and by cryoelectron microscopy. In such micrographs, the two species could be unambiguously distinguished and counted. All three methods showed good agreement (Figures 3−5; Table 1). Moreover, the choice of assembly method, mixing or dialysis (see Materials and Methods), did not affect the efficiency of assembly nor the ratio of $T = 3$ to $T = 4$ particles obtained.

The proportion of $T = 4$ capsids decreased progressively as the protein construct was shortened from its C-terminus.

FIGURE 3: Cryoelectron micrographs comparing $T = 3$ and $T = 4$ capsid populations separated on sucrose gradients to the mixture that is produced upon *in vitro* assembly of Cp142. (a) Freshly assembled Cp142 contains 51% of $T = 4$ capsids ($n = 1121$). (b) $T = 3$ capsids, gradient-purified from the same Cp142 sample shown in panel a. The content of contaminating $T = 4$ particles is only 3% ($n = 3118$). (c) This preparation of gradient-purified $T = 4$ capsids, also from the same Cp142 sample, retains about 10% $T = 3$ capsids ($n = 3731$). This latter sample represents a high level of contamination compared to most preparations which typically contain <5% of the contaminating form of capsid. Scale bar = 50 nm.

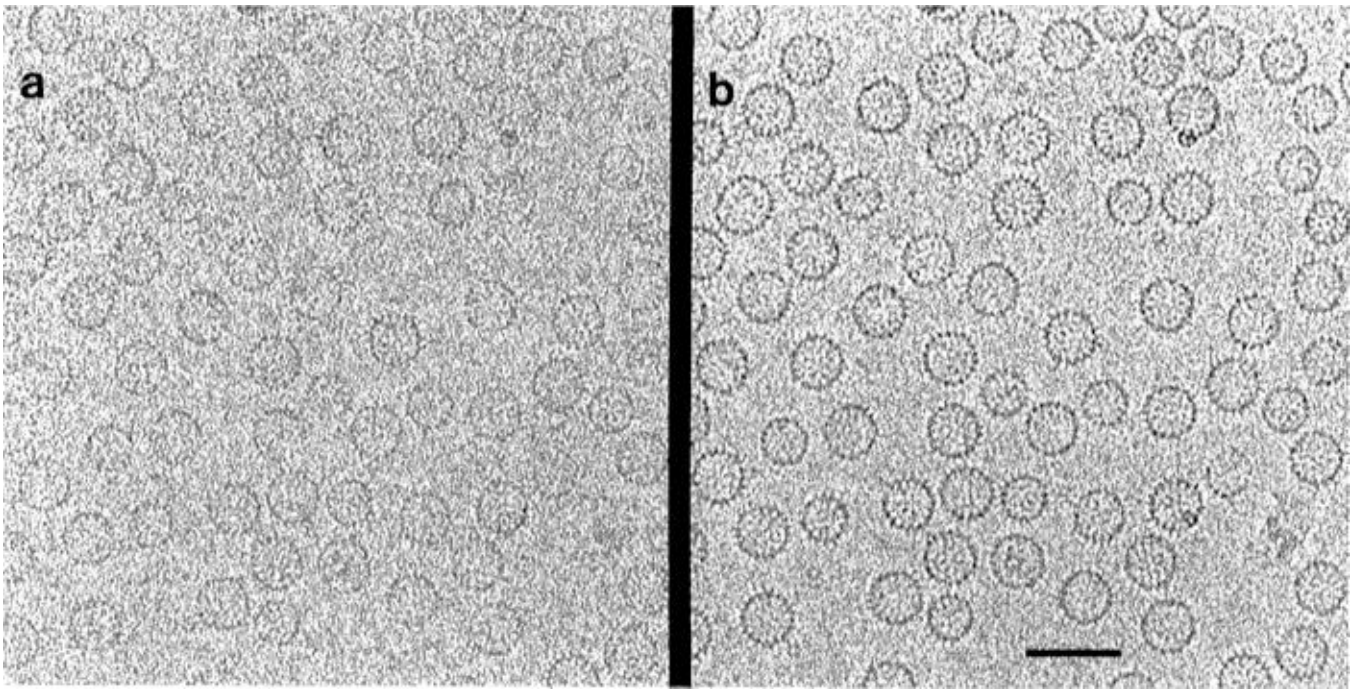

FIGURE 5: Focal pair of cryoelectron micrographs of Cp147 used to calculate the three-dimensional image reconstructions. The field shown corresponds to about 5% of the micrograph. The closer-to focus micrograph (a) has its first CTF zero at a spatial frequency of (17 Å)$^{-1}$. The further-from-focus micrograph (b) has its first zero at (28 Å)$^{-1}$. The scale bar is 50 nm.

Table 1: Percentage of $T = 4$ Capsids for Different Cp Variants[a]

	sucrose gradient	analytical ultracentrifugation	cryo-EM
Cp149	79 ± 8	96	94 (3414)
Cp147	66 ± 7	nd[b]	79 (4673)
Cp142	56 ± 5	50	51 (1121)
Cp140	18	20	nd
Cp138	no assembly		
Cpe	13 ± 6	16	15 (2992)
Cp149 C61A	63	69	nd

[a] For gradients and analytical centrifugation analyses, the reported percentages of $T = 4$ capsids were calculated from the measured amounts of protein, $M_{T=4}$ and $M_{T=3}$, by $\%_{T=4} = 100[0.75M_{T=4}]/[M_{T=3} + 0.75M_{T=4}]$. Standard deviations, from at least four experiments, are reported for the percentages determined by sucrose gradient. The parenthetical values in the cryo-EM column are the total number of particles counted. [b] nd, not determined.

Cp149 capsids were predominantly (>90%) $T = 4$, whereas for Cp140 only about 15% of the capsids were of this form. For Cp149 and Cp147, the proportions of $T = 3$ capsids estimated from sucrose gradients were somewhat higher than those determined by cryoelectron microscopy (and, for Cp149, by analytical ultracentrifugation). This discrepancy probably arises from the difficulty in visualizing and isolating a faint $T = 3$ band in the presence of a dense $T = 4$ band, resulting in a larger margin of error. Thus we consider that the cryoelectron microscopy and analytical ultracentrifugation data yield more reliable values for these two experiments.

Other modifications to the protein sequence also affected the proportions of $T = 4$ and $T = 3$ capsids (Table 1). Cpe is C-terminally truncated at residue 144 but has a lower $T = 4$ content than would be expected from the trend described above. However, it has several additional amino acids extending its N- and C-termini. Cp149 C61A is the same length as Cp149 but produces more $T = 3$ capsids. This protein contains a mutation to alanine of cysteine 61, which can form an intermolecular disulfide crosslink between half-dimers (Zheng et al., 1992; Nassal et al., 1992).

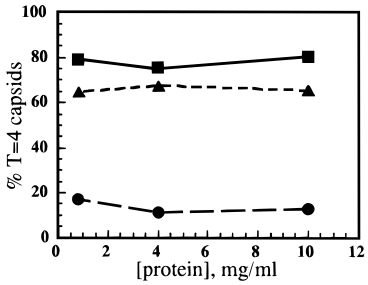

FIGURE 6: Concentration dependence of the proportion of $T = 4$ capsids. The percentage of $T = 4$ capsids, determined using sucrose gradients, is shown as a function of the initial protein concentration for Cp149 (—), Cp147 (- - -), and Cpe (— — —).

The Proportions of $T = 4$ and $T = 3$ Particles Are Not Concentration-Dependent. The different numbers of dimers in $T = 3$ and $T = 4$ particles, 90 compared to 120, suggested that protein concentration may play some role in size determination (Zlotnick, 1994). To test this hypothesis, the ratio of $T = 3$ to $T = 4$ was determined for capsids assembled at concentrations of 0.8−10 mg/mL. This range was limited by the considerations that assembly should be nearly quantitative and only initiated by adjusting conditions to high ionic strength and neutral pH. At least 0.5 mg/mL is needed for efficient assembly (Wingfield et al., 1995; Seifer et al., 1993), and above 20 mg/mL some Cp proteins assemble, even in 0.1 M bicarbonate, pH 9.5. These experiments were performed for three proteins: Cp149, Cp147, and Cpe. In all cases, the fractions of $T = 4$ capsids remained fixed at ~80%, 65%, and 15%, respectively, as determined from sucrose gradients (Figure 6).

Cryoelectron Microscopy and Image Reconstructions. The two differently sized capsids were easy to distinguish in cryoelectron micrographs for the assembly products of any of the proteins studied (e.g., Figures 3 and 5). The larger particles were ~300 Å in diameter, and the smaller were ~260 Å. Some features could be discerned directly on the

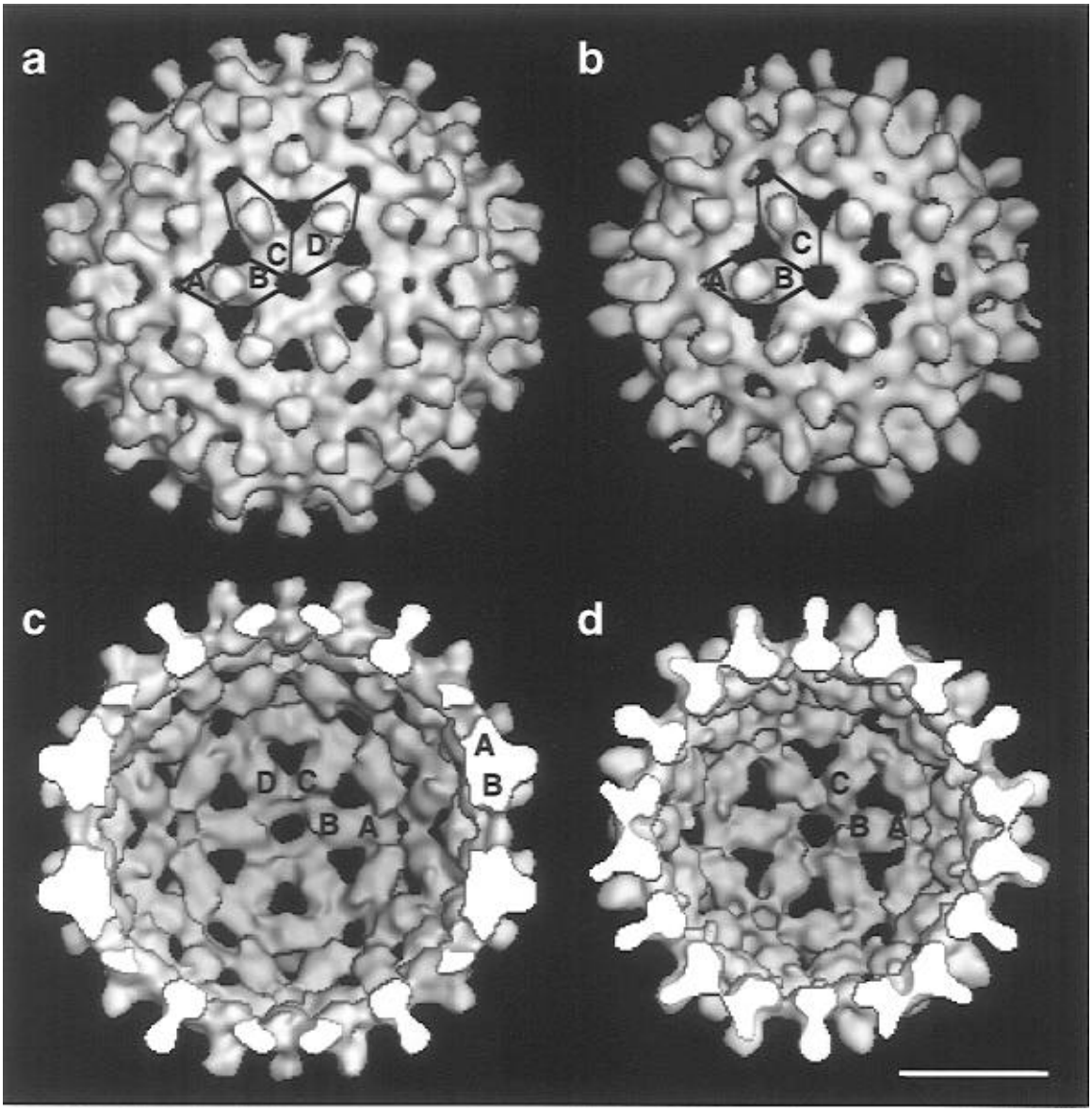

FIGURE 7: Image reconstructions of Cp147 capsids showing icosahedral quasi-six-fold axes. Subunits (half-dimers) are designated as A, B, C, and D for the $T = 4$ capsid (a, c) and A, B, and C for the $T = 3$ (b, d) (see Figure 2). (a) The $T = 4$ quasi-six-fold axis coincides with the icosahedral two-fold axis. (b) The $T = 3$ quasi-six-fold axis coincides with the icosahedral three-fold axis. Only the front half of each particle is rendered in the exterior views to avoid obscuring the holes that perforate the capsids. (c) Interior view of the $T = 4$ capsid. The cutaway view exposes a cross section of the AB dimer. A cross section of the small cavity found along the five-fold axis (see text) can be seen adjacent to the cutaway view of the A subunit. (d) Interior view of the $T = 3$ capsid. Both the $T = 3$ and the $T = 4$ reconstructions were contoured to include a volume equal to 100% of the protein, assuming a specific volume of 0.742 cm^3/g. Scale bar = 100 Å (10 nm).

micrographs, notably a fringe of small projections around the peripheries of both large and small capsids. A small number of bacilliform capsids were observed. Many of these were ~260 Å in diameter and up to ~300 Å long and may represent misassembled or damaged $T = 3$ particles.

Density maps were calculated from micrographs of capsids assembled from Cp147 (Figure 5). With this protein, enough capsids of both kinds may be found in the same micrograph to allow reconstructions of both to be calculated. In these circumstances, differences in structural detail between the $T = 3$ and $T = 4$ capsids cannot be attributed to microscopy-related factors, such as differences in defocus (despite the CTF correction), ice thickness, specimen movement, etc. As expected, the reconstructions of the large and small capsids revealed $T = 4$ and $T = 3$ symmetry, respectively (Figure 7). In terms of overall structure, both capsids consist of a fenestrated contiguous shell, studded with radially protruding spikes. The dimensions of both capsids were measured from our reconstructions, as calculated to 17 Å resolution from micrographs of calibrated magnification and contoured to enclose 100% of the expected mass. For the $T = 4$ capsid, the maximum outer radius is 174 Å at the tip of the AB spike; the inner radius, from beneath the AB dimer axis, is 125 Å. The corresponding figures are 159 and 107 Å, respectively for the $T = 3$ particle. The length of the spikes is 28 Å, from the outer radius to the contiguous shell (see below), and is the same for both capsids.

Structures of Dimers and Half-Dimers. The structures visualized in our reconstructions are fully consistent with the observation made in solution studies that the fundamental building block is a dimer of capsid protein (Wingfield et al., 1995). The dimer is shaped like an inverted capital "T". The cross-pieces of the T's, which are ~70 Å long and ~30 Å wide, pack together to form the contiguous shell. Their ends are bivalent and are arranged to form five- and six-membered rings at the five-fold and quasi-six-fold axes,

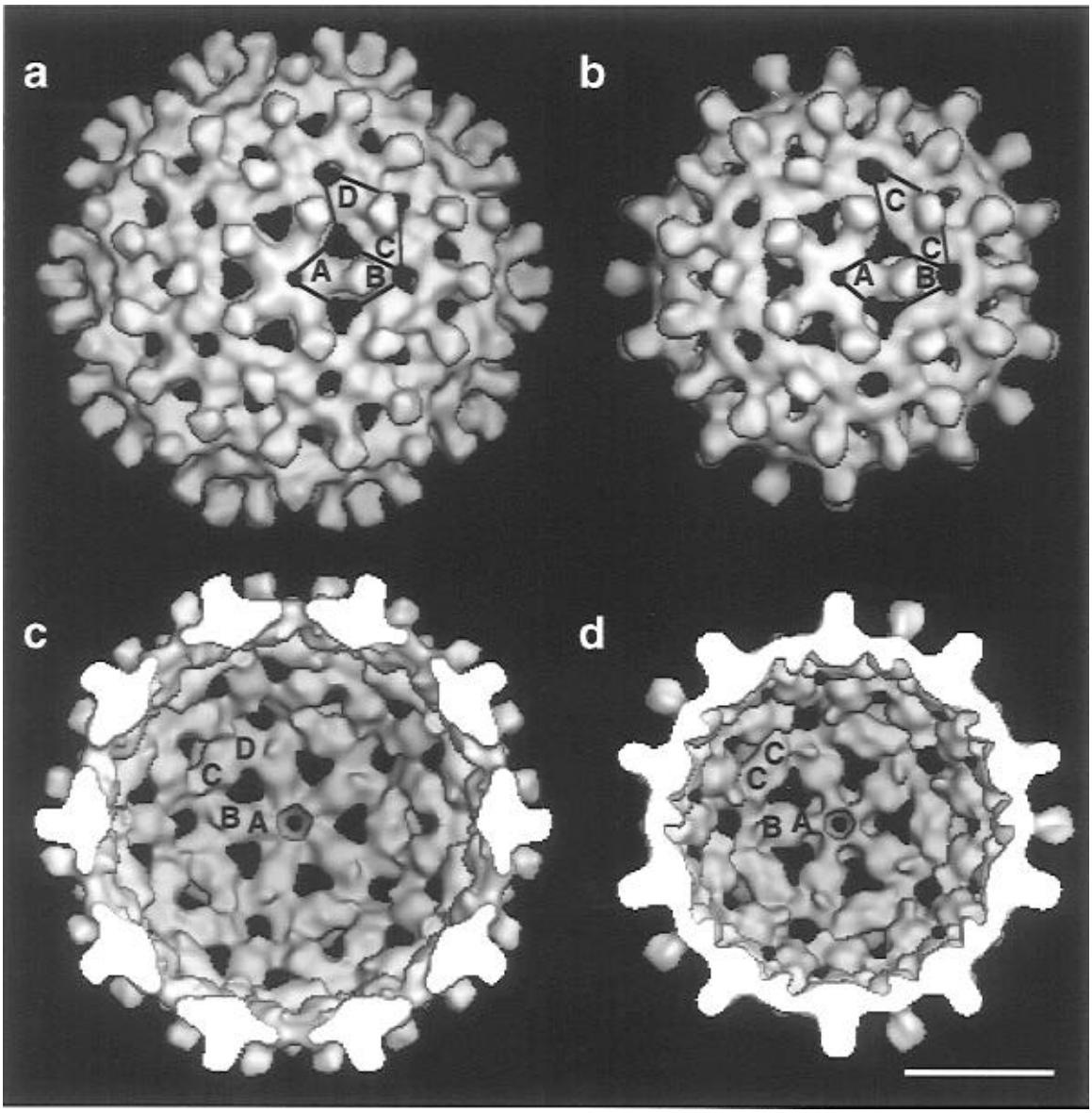

FIGURE 8: Image reconstructions of Cp147 capsids. Exterior and interior views along the icosahedral five-fold axes of the $T = 4$ capsid (a, c) and $T = 3$ capsid (b, d). Images are contoured as in Figure 7.

respectively. Ridges and grooves on the interior and exterior surfaces of the capsids, which are not evident at 30 Å resolution, indicate the likely boundaries between adjacent dimers (Figure 7).

The stems of the T's form the external spikes which are located on two-fold and quasi-two-fold axes (Figures 7 and 8). The spikes are knob-like, tapering to a neck that is indented on both sides, as they approach the contiguous shell. The volume of each spike corresponds to a mass of ~7300 Da, assuming a partial specific volume of 0.742 cm^3/g for the capsid protein. The spikes are very similar in structure for all four types of dimer (i.e., $T = 3$ AB and CC and $T = 4$ AB and CD; see Figure 2 for a definition of this labeling of subunits in different quasi-equivalent environments).

Interior views of the dimers (Figures 7 and 8) show that they are roughly diamond-shaped with distinct two-fold symmetry. We note that the AB and CD dimers are not constrained to have this symmetry by the icosahedral symmetry imposed in the reconstruction procedure. A small protrusion is found at either end of the diamond for all seven classes of half dimer ($T = 3$: A, B, and C. $T = 4$: A, B, C, and D). This protrusion can also be seen in the cross sections through the $T = 4$ AB dimer shown in Figure 7c. At our current resolution of 17 Å, the half-dimers in all seven geometrically distinct environments (see Figure 2) look very similar.

Quaternary Structures Surrounding the Five-Fold and Quasi-Six-Fold Axes. The arrangement of dimers around the icosahedral five-fold axis is virtually identical in the $T = 3$ and $T = 4$ particles (Figure 8). Cross-sections through the AB dimers of the respective capsids are superimposable (not shown). Small holes, ~10 Å in diameter, not seen at lower (~30 Å) resolution, are present at the five-fold axes of both capsids. These holes widen into cylindrical cavities, ~22 Å in diameter, recessed into the inner surface of the capsid wall (Figures 7c, and 8c,d).

There are also holes at the quasi-three-fold sites surrounding the five-fold axes. These holes are enclosed by two AB dimers and one CC or CD dimer. The longest chord for these holes is 25 Å for $T = 4$ and 32 Å for $T = 3$ capsids (see Table 2). The $T = 4$ capsid has a third class of triangular hole at the three-fold axis, formed by the three CD dimers,

Table 2: Numbers and Areas of Holes Perforating HBV Capsids[a]

	$T = 3$				$T = 4$			
hole sites	no.	D_1 (Å)	D_2 (Å)	area (Å^2)	no.	D_1 (Å)	D_2 (Å)	area (Å^2)
five-fold axis	12	10	10	80	12	10	10	80
quasi-six-fold axis	20	22	22	330	30	24	18	330
between AB dimers (quasi-three-fold axes)	60	32	28	500	60	25	25	450
between CD dimers ($T = 4$ three-fold axis)					20	27	22	390

[a] D_1 is the length of the longest vector across a hole, and D_2 is the length of the vector perpendicular to D_1. The size of the holes depends on the choice of contour level and the depth within the contiguous shell at which they are measured. These dimensions were measured from a model contoured to enclose 100% of expected mass and at the narrowest points of the holes, i.e., at a radius of 130 Å for the $T = 3$ particle and 150 Å for the $T = 4$ particle. The shapes of the holes (e.g., the D_1/D_2 ratio) is less sensitive to the contour level used.

very similar to those on the quasi-three-fold axes. Cumulatively, holes occupy ~16% of the surface area of both the $T = 3$ and $T = 4$ capsids.

Although the structures around the five-fold axes of $T = 4$ and $T = 3$ capsids are essentially identical, there are distinct differences in the vicinity of the quasi-six-fold axes (Figure 7). Six-fold symmetry is more closely approximated in the $T = 3$ than in the $T = 4$ capsid. This is evident in the shape of the central hole: whereas the $T = 3$ quasi-six-fold hole is roughly circular (~22 Å diameter), the $T = 4$ hole is oval, ~24 Å long by 18 Å wide. In both capsid types, the quasi-six-fold related dimers are not coplanar. The long axis of the AB dimers (extending from the quasi-six-fold to five-fold), two for $T = 4$ quasi-six-fold and three for $T = 3$, are closer to perpendicular to the quasisymmetry axes than are the corresponding axes for CC or CD dimers (for a cross section of $T = 4$ AB dimers, see Figure 8d). This results in the impression that the AB spikes are closer to the quasi-six-fold axes than the CC and CD spikes.

DISCUSSION

We have investigated dimorphism in the assembly of HBV capsids, using physicochemical techniques and structural analysis by cryoelectron microscopy and image reconstruction to characterize capsids produced by a range of mutant constructs. Our major finding is that a relatively short segment of the C-terminus, between residues 138 and 149, inclusive, plays a critical role in dictating (i) whether the protein will be assembly-competent (residues 138−140), and (ii) whether it will produce predominantly $T = 3$ or $T = 4$ capsids (residues 140−149). Residues distal to amino acid 149 have little effect on the dimorphic switch in that a large majority of Cp149 capsids are $T = 4$, as with HBcAg capsids assembled in *E. coli* (Crowther et al., 1994; Wingfield et al., 1995) and native capsids isolated from infected human livers (Kenney et al., 1995). However, the phenotypes of the Cpe and Cp149 C61A mutations indicate that the C-terminus is not the only factor to affect the dimorphism.

Assembly and Dimorphism of Capsid Protein Dimers. The observation that the C-terminus is an important determinant of assembly raises the questions of where this moiety is located on the T-shaped dimer and how its influence on capsid size is imposed. In principle, assembly incompetence caused by removal of residues 139 and 140 could come about by rendering the polypeptide chain unable to fold, by preventing dimerization, or by preventing dimers from assembling. At present, we are unable to settle this issue because the folding and oligomeric status of Cp138 is unclear. When this protein is expressed in bacteria, it forms large inclusion bodies from which it may be extracted only by extreme denaturing treatments (P.W. and S.S., unpublished results).

If the basic C-terminus (distal to residue 149) is present, as in HBcAg, this moiety binds nucleic acids that line the inner surface of the capsid (Crowther et al., 1994; Wingfield et al., 1995). It follows that the adjacent residues 140−149 are likely also to be on or close to the inner surface. Kenney et al. (1995) observed additional density underlying the HBcAg dimer interfaces, which they suggested might be part of the C-terminus. This site is a plausible one, as residues in this locality are strategically placed to affect how the two monomers that make up a dimer interact. However, the alternative possibility that the observed density might represent nucleic acid attaching to some charged patch on the inner surface does not seem to be ruled out.

Structural Features of the Capsids. At 30 Å resolution, our reconstructions have the same general features as those described by Crowther et al. (1994), although we find the holes to be significantly larger: for example, the $T = 3$ quasi-six-fold hole is 22 Å in diameter in our reconstruction compared to ~14 Å diameter [as measured from the surface shaded map shown in Crowther et al. (1994)]. This distinction may reflect the contouring criteria applied in the respective studies (see Results). Upon extension of the resolution to 17 Å, further details become apparent. In particular, the holes at the quasi-six-fold axes of the $T = 4$ capsid are seen to have a markedly elongated shape. The larger number and size of the holes revealed in this study have functional implications. The HBV capsid serves as a biosynthetic compartment for retrotranscription and expression of the genome: that the capsid is considerably more porous than has been previously appreciated helps explain the ready ingress of substrate nucleotides and egress of digested RNA.

Also, at 17 Å resolution, the arrangement of dimers around the quasi-six-fold axis of the $T = 4$ capsid is visibly different from that of the $T = 3$ capsid. In both capsids, the spikes of the AB dimers appear closer to the quasi-six-fold symmetry axis than the CC or CD spikes. This is because the AB dimers are more nearly perpendicular to the symmetry axis than the CC or CD dimers. In addition, the contact between the adjacent CD dimers around the quasi-six-fold axis of the $T = 4$ capsid help to give it an elongated appearance (Figure 7).

From the calculated volume of the protruding spikes, we estimate that they receive a contribution of about 35 amino acids from each monomer. The high α-helical content of the capsid protein and the dimensions of the spike (~28 Å long with a 27 by 20 Å cross section at half height) suggest the possibility that the spike consists of an α helical bundle (Weber & Salemme, 1981; Harris et al., 1994) with each monomer contributing two antiparallel α-helices, each ~15 residues long, connected by a turn. In principle, such helices could extend further along the dimer interface into the contiguous shell.

Another new feature is the very small protrusion at either end of the diamond-shaped inner surface of the dimer

(Figures 7 and 8). From its estimated volume, the mass contained should be less than 1 kDa. Nevertheless, because it is reproducibly observed in subunits that are not related by symmetry and in both the $T = 3$ and $T = 4$ structures, we consider that it is genuine and most likely represents a surface loop. We note that comparably small features have been reported in cryoelectron microscopic reconstructions of bacteriophage ϕ X174 at 20 Å resolution (Ilag et al., 1995).

Capsid Assembly and the Regulation of Dimorphism. The following two observations bear on the mechanism of assembly. (i) The absence of equilibration between $T = 3$ and $T = 4$ capsids indicates that dimorphism is controlled at a kinetic level. (ii) The lack of concentration dependence or rather, the zero power concentration dependence of the $T = 3/T = 4$ capsid ratio, suggests both forms assemble either from a common initiation complex or from complexes that are the same size. A quasi-six-fold arrangement of dimers, the site of the greatest difference in quaternary structure, could play an important role in such a complex by adopting either $T = 3$ or $T = 4$ conformations.

An alternative mechanism is that subunits in the pool of unassembled dimers transiently adopt conformations which influence the form of capsid to be produced. In this sort of "subunit-based" mechanism, the proportion of $T = 4$ capsids could be controlled by influencing the concentration of subunits in $T = 4$ C or D conformations, as opposed to A, B, or $T = 3$ C forms. In this scenario, the effect of C-terminal truncations would be to reduce the propensity of the subunits for the $T = 4$ conformations. Both the "subunit-based" and the "complex-based" mechanisms are consistent with the lack of concentration dependence of the $T = 3/T = 4$ ratio and the pronounced differences in the local structure of $T = 3$ and $T = 4$ capsids around the quasi-six-fold axes.

ACKNOWLEDGMENT

We are grateful to Mr. Ira Palmer and Mr. Joshua Kaufman for their contributions to producing and purifying the large amounts of protein used in this study. We also wish to acknowledge many helpful discussions with Dr. Benes Trus.

REFERENCES

Baker, T. S., Drak, J., & Bina, M., (1988) *Proc. Natl. Acad. Sci. U.S.A. 85*, 422−426.
Baker, T. S., Drak, J., & Bina, M. (1989) *Biophys. J. 55*, 243−253.
Baker, T. S., & Cheng, R. H. (1996) *J. Struct. Biol. 116*, 120−130.
Banks, S. (1990) in *Signal Processing, Image Processing, and Pattern Recognition*, pp 215−219, Prentice Hall Inc., Englewood, NJ.
Bartenschlager, R., & Schaller, H. (1992) *EMBO J. 11*, 3413−3420.
Beames, B., & Landford, R. E. (1993) *Virology 194*, 597−607.
Birnbaum, F., & Nassal, M. (1990) *J. Virol. 64*, 3319−3330.
Booy, F. P., Ruigrok, R. W., & van Bruggen, E. F. (1985) *J. Mol. Biol. 184*, 667−676.
Booy, F. P., Newcomb, W. W., Trus, B. L., Brown, J. C., Baker, T. S., & Steven, A. C. (1991) *Cell 64*, 1007−1015.
Caspar, D. L. D., & Klug, A. (1962) *Cold Spring Harbor Symp. Quant. Biol. 27*, 1−24.
Cohen, B. S., & Richmond, J. E. (1982) *Nature 296*, 677−678.
Conway, J. F., Trus, B. L., Booy, F. P., Newcomb, W. W., Brown, J. C., & Steven, A. C. (1993) *J. Struct. Biol. 111*, 222−233.
Coombs, D. H., & Watts, N. (1985) *Anal. Biochem. 148*, 254−259.
Crowther, R. A. (1971) *Phil. Trans. R. Soc. London B 261*, 221−230.
Crowther, R. A., Kiselev, N. A., Böttcher, B., Berriman, J. A., Borisova, G. P., Ose, V., & Pumpens, P. (1994) *Cell 77*, 943−950.
Frank, J. Zhu, J., Penczek, P., Li, Y., Srivastava, S., Verschoor, A., Radermacher, M., Grassucci R., Lata, R K., & Agrawal, R K. (1995) *Nature 376*, 441−444.
Fuller, S. D. (1987) *Cell 48*, 923−934.
Ganem, D., & Varmus, H. E. (1987) *Annu. Rev. Biochem. 56*, 651−693.
Harris, N. L., Presnell, S. R., & Cohen, F. E. (1994) *J. Mol. Biol. 236*, 1356−1368.
Hollinger, F. B. (1990) in *Virology* (Fields, B. N., & Knipe, D. M., Eds.) pp 2171−2236, Raven Press, Ltd., New York.
Ilag, L. L., Olson, N. H., Dokland, T., Music, C. L., Cheng, R. H., Bowen, Z., McKenna, R., Rossmann, M. G., Baker, T. S., & Incardona, N. L. (1995) *Structure 3*, 353−363.
Johnson, C. A., Weisenfeld, N. I., Trus, B. L., Conway, J. F., Martíno, R. L., & Steven, A. C. (1994) in Proceedings of the Supercomputing 94, pp 550−559, IEEE Computer Society, Los Alamítos.
Kenney, J. M., von Bonsdorff, C.-H., Nassal, M., & Fuller, S. D. (1995) *Nature Struct. Biol. 3*, 1009−1019.
Misell, D. L. (1978) *Image Analysis, Enhancement, & Interpretation.* Elsevier/North Holland Inc., New York.
Moody, M. F., & Makowski, L. (1981) *J. Mol. Biol. 150*, 217−244.
Murray, K. (1987) *Proc. R. Soc. London B230*, 107−146
Nassal, M., & Schaller, H. (1993) *Trends Microbiol. 1*, 221−228.
Nassal, M., Rieger, A., & Steinau, O. (1992) *J. Mol. Biol. 225*, 1013−1025.
Pasek, M., Goto, T., Gilbert, W., Zink, B., Schaller, H., Mackay, P., Leadbetter, G., & Murray, K. (1979) *Nature 282*, 575−579.
Petit, M. A., & Pilot, J. (1985) *J. Virol. 53*, 543−551.
Robinson, W. S. (1991) in *Virology* (Fields, B. N., & Knipe, D. M., Eds.) pp 989−1021, Raven Press, Ltd., New York.
Rossmann, M. G., & Johnson, J. E. (1989) *Annu. Rev. Biochem. 58*, 533−573.
Saxton, W. O., & Baumeister, W. (1982) *J. Microsc. 127*, 127−138.
Scharf, S. J., Horn, G. T., & Erlich, M. A. (1986) *Science 233*, 1076−1078.
Schachman, H. K. (1959) *Ultracentrifugation in Biochemistry*, Academic Press, New York.
Seifer, M., Zhou, S., & Standring, D. N. (1993) *J. Virol. 67*, 249−257.
Stafford, W. F. (1992) *Anal. Biochem. 203*, 295−301.
Stahl, S. J., & Murray, K. (1989) *Proc. Natl. Acad. Sci. U.S.A. 86*, 6283−6287.
Stahl, S., Mackay, P., Magazin, M., Bruce, S. S., & Murray, K. (1982) *Proc. Natl. Acad. Sci. U.S.A. 79*, 1607−1610.
Stuart, D. I. (1993) *Curr. Opin. Struct. Biol. 3*, 167−174.
Studier, F. W., Rosenberg, A. H., Dunn, J. J., & Dobendorff, J. W. (1990) *Methods Enzymol. 185*, 60−89.
Summers, J., & Mason, W. S. (1982) *Cell 29*, 403−415.
Takahashi, K., Machida, A., Funatsu, G., Nomura, M., Usuda, S., Miyakawa, Y., & Mayumi, M. J. (1983) *Immunology 130*, 2903−2907.
Toyoshima, C., & Unwin, N. (1988) *Ultramicroscopy 25*, 279−291.
Trus, B. L., Newcomb, W. W., Booy, F. P., Brown, J. C., & Steven, A. C. (1992) *Proc. Natl. Acad. Sci. U.S.A. 89*, 11508−11512.
Unwin, N. (1993) *J. Mol. Biol. 229*, 1101−1124.
Weber, P. C., & Salemme, F. R. (1981) *Nature 287*, 82−84.
Wingfield, P. T., Stahl, S. J., Williams, R. W., & Steven, A. C. (1995) *Biochemistry 34*, 4919−4932.
Zheng, J., Schödel, F., & Peterson, D. L. (1992) *J. Biol. Chem. 267*, 9422−9429.
Zhou, Z. H., Prasad, B. V., Jakana, J., Rixon, F. J., & Chiu, W. (1994) *J. Mol. Biol. 242*, 456−469.
Zlotnick, A. (1994) *J. Mol. Biol. 241*, 59−67.

BI9604800